

https://dspace.org/

Fracture Mechanics Analyses Of Static And Dynamic Failures Associated With Welding

Boothroyd, Colin Allistair

2015-01-09
http://hdl.handle.net/10539/16336

Downloaded from a DSpace repository. https://dspace.org/

from the radiographs, taken before the start of the UT programmes.

2.3.3. The second inspection programme

Following the line of the previous discussion, it was felt that the preliminary findings did not truly represent the level of competence of the ultrasonic personnel involved in the inspections, and since the initial aim of this work was not to discredit ultrasonic defect sizing in general, but to obtain a better understanding of the reliability and limitations of this valuable engineering tool, a further validation exercise was initiated, on the remaining ten test plates. In this second "round-robin" inspection programme, the operators were told that the defects were due to lack of penetration, and therefore aligned perpendicularly to the plate surfaces, coincident with the weld centre-line (marked indelibly on each of the plates).

The operators were therefore asked to measure and record the distance between the top surface of the plate and the top of the defect, at three locations across the width of the weld. They were then asked to repeat this procedure from the bottom surface of the plate. It had been decided that three readings should be taken from either surface, since it had been observed from the fracture surfaces of the twenty test plates that had already been destructively tested that, in some cases, the top and bottom defect edges were not parallel with each other, or with the top and bottom surfaces of the test plates, as had originally been designed.

The operators were again chosen such that they represented a broad spectrum of previous experience in practical ultrasonic examination. Furthermore this group included Operator D, who was observed to be one of the more accurate inspectors in the initial test programme, and Operator R who had been one of the least accurate. While it was expected that the accuracy of both these inspectors would increase in the second test series, it was hoped that the disparity between them would be reduced.

The results obtained are summarised in Figures 2.16 to 2.18, and these should be compared to the corresponding results of the first test programme (compare Figure 2.16 with Figure 2.7, and Figure 2.18 with Figure 2.5). It is evident that a substantial increase in the accuracy of defect sizing was achieved, and furthermore the ultrasonic predictions of defect height tend to increase with the actual defect heights.

For this second series of inspections, it was indicated that an error of 1,5mm could be expected on the two depth measurements, and this would give rise to a cumulative error of 3mm on defect height predictions. Accordingly, the number of times each operator predicted a defect height within 3mm of the actual defect height was compared to the number of times that operator undersized or oversized the defect. This is shown schematically in Figure 2.19, which should be compared to Figure 2.14. Again, this comparison illustrates the increased accuracy that was achieved in the second test programme, with the least accurate operator correctly sizing seven of the ten defect heights. Furthermore, operator D, who was one of the most experienced inspectors, with 28 years in this field, correctly sized all ten of the defects, and operator R who was one of the least accurate in the initial test programme sized eight of the ten defects within the 3mm error range.

It will be seen from Figure 2.19 that there is again a slight tendency to underestimate the defect heights (11 of the 120 predicted defect heights were undersized, whereas 7 were oversized), but this trend is not quite as evident as in the first inspection programme.

2.4 Summary

This Chapter has reviewed the common NDT methods, and outlined the applicability, advantages and disadvantages of each method. While it appears that ultrasound techniques are the most versatile, and can be used to detect and

size all defect types, it is clear that even these methods have limitations.

The results obtained in the two ultrasonic test programmes performed on artificial defects in fusion welded joints were detailed. Initial results were very poor and considerable variability, both between operators and between predicted and actual defect parameter was observed. There was a general tendency to undersize defect lengths and heights, while the apparent trend in oversizing defect depths could have arisen due to undersizing the heights.

No clear cut correlations between operator experience and accuracy emerged, apart from the observation that the two inspectors with twenty years experience tended, on the whole, to be more consistently accurate than the less experienced operators.

The marked disparity in defect size predictions was suggested to have arisen primarily from the nature of the defects. Although these defects had originally been designed to be large (in relation to the weld dimensions) so as to aid the ultrasonic inspections, they were in fact in excess of any code requirement. Thus, in a practical situation, the operators would reject such a defect rather than attempt to size it. Additionally the machined root face of these manufactured defects gave a reduced signal intensity relative to that reflected from the edges, and it was shown how this could give rise to substantial errors in predictions of defect height (and therefore, depth). However, it is worth reiterating that the operators were somewhat optimistic in their predicted errors, which is suprising when the above factors are considered.

The twelve operators involved in the second test programme obtained a far greater accuracy in predictions of defect parameters. These results indicated that if a series of unknown, but different sized defects were ultrasonically inspected, then the range in the UT predictions would give some indication of the relative extent of the defects. These results however, are contingent on the inspectors being given sufficient information about the defect, and provided

with a specified sizing procedure.

Table 2.1 : Specified chemical compositional ranges and mechanical properties of ROQ-tuf AD 690.

Element	Specified weight %
C	0,12-0,21
Mn	0,45-0,70
Si	0,20-0,35
P	0,35 (max)
S	0,04 (max)
Mo	0,50-0,65

Yield Stress	690 MPa (min)
Tensile Strength	760-895 MPa

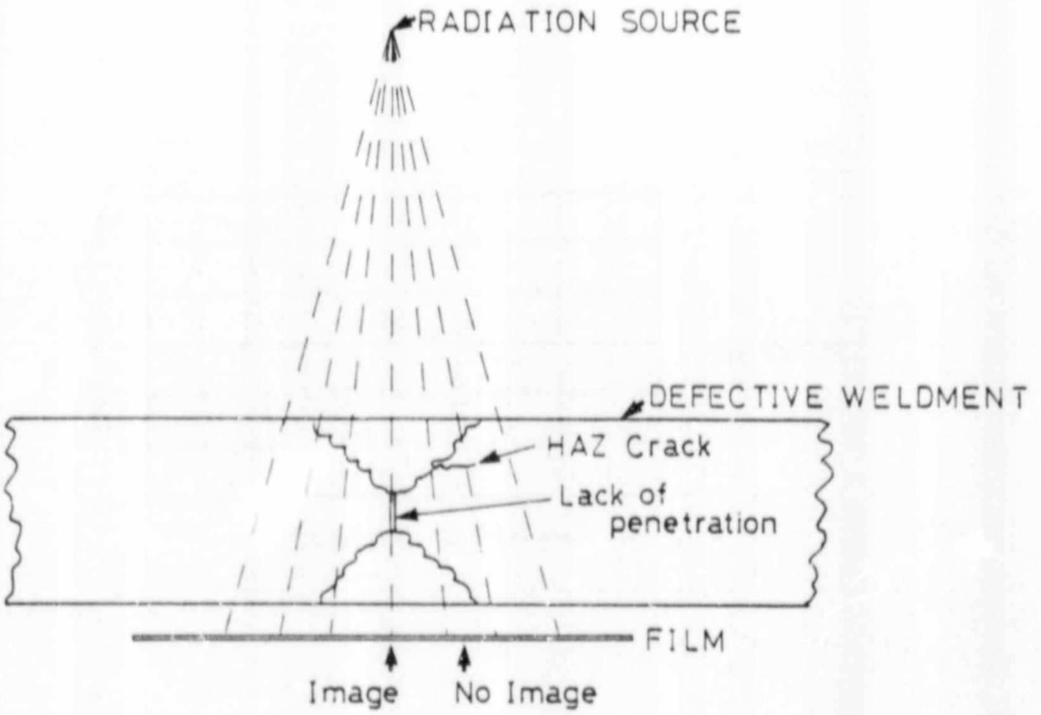


Figure 2.1 A schematic illustration of the limitations of radiographic techniques for detecting planar defects.

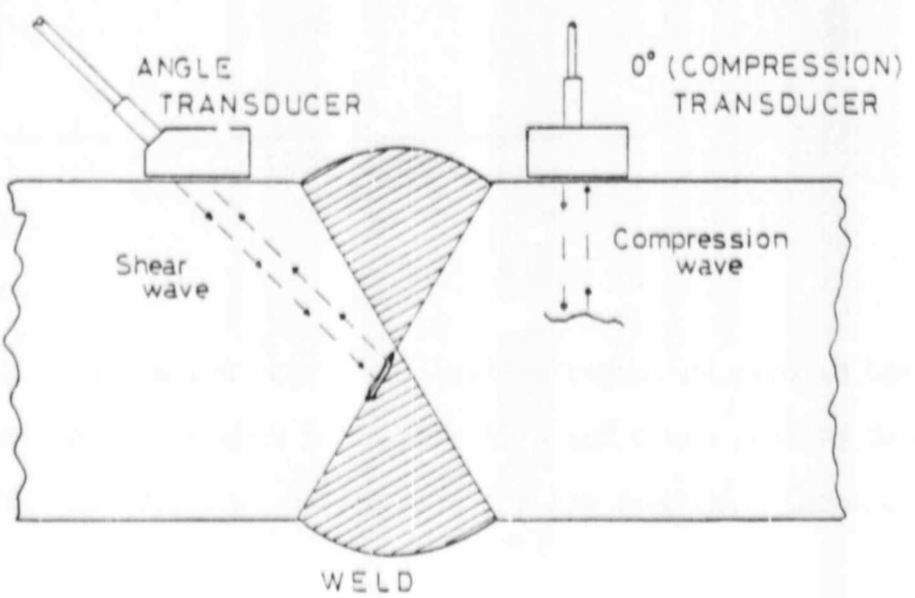


Figure 2.2 A schematic of a UT inspection, indicating how the type of flaw influences the probe type.

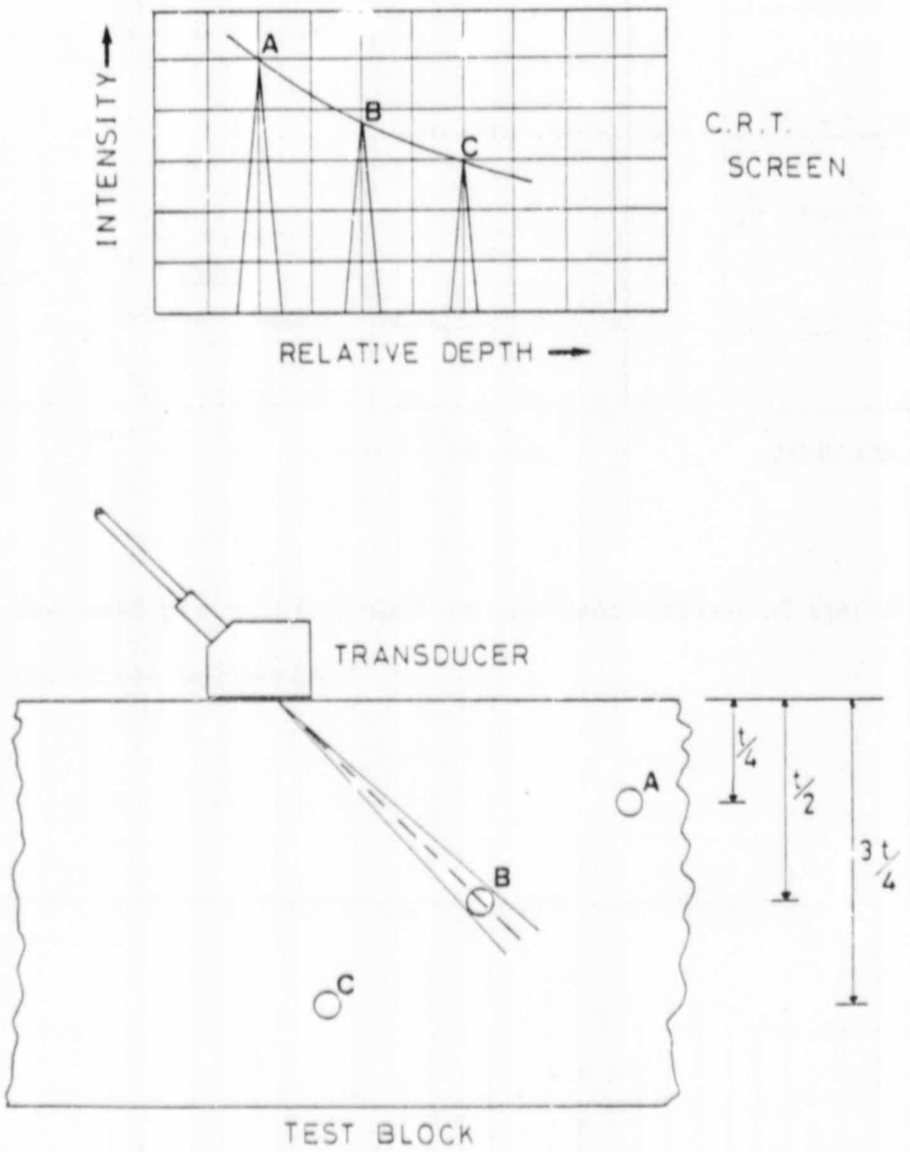


Figure 2.3 An illustration of the calibration technique used in the DAC method. Reference reflectors A, B and C are usually determined from the critical defect size for the component inspected.

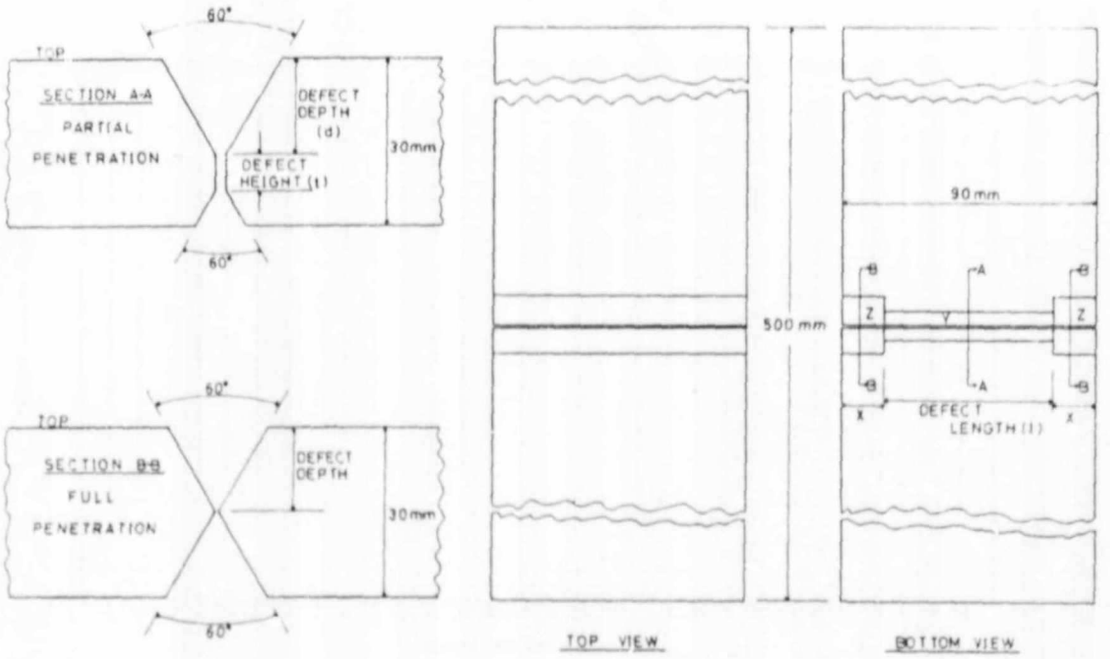


Figure 2.4 The weld preparation used in the fabrication of the defective weldments.

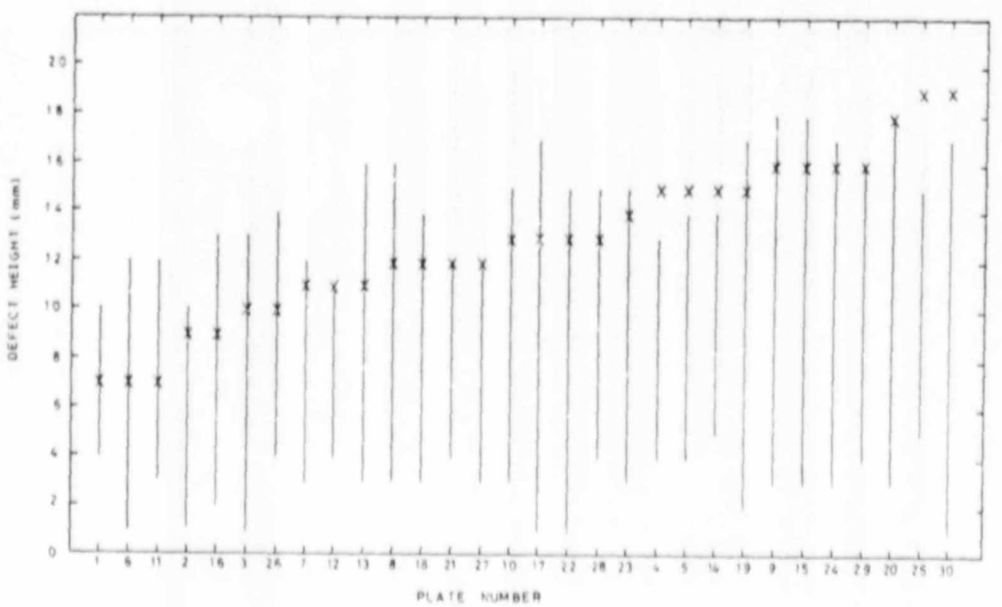


Figure 2.5 The range in UT predictions of defect heights. (Actual defect height indicated by X).

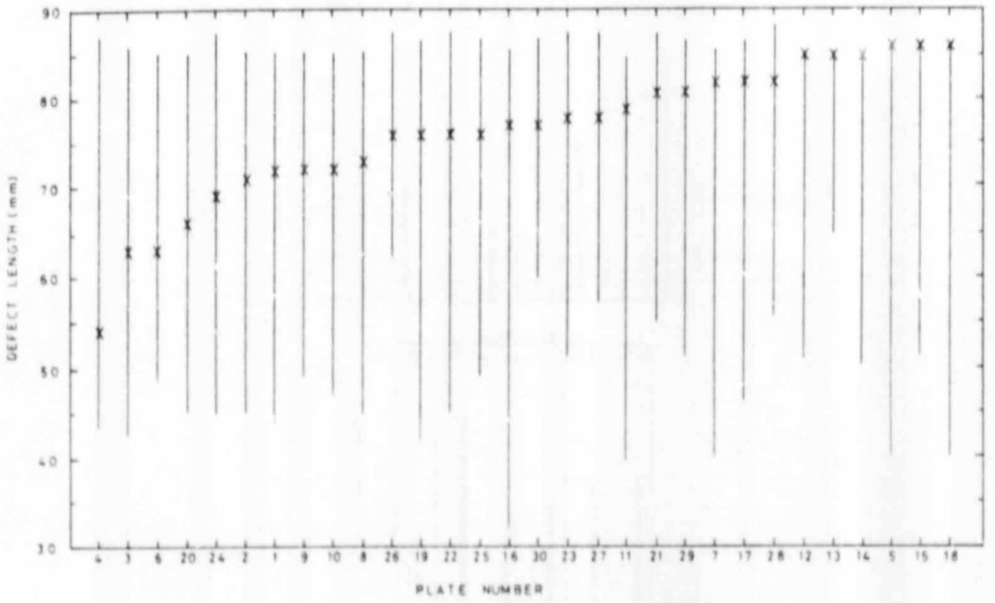


Figure 2.6 The range in UT predictions of defect lengths. (Actual defect length indicated by X).

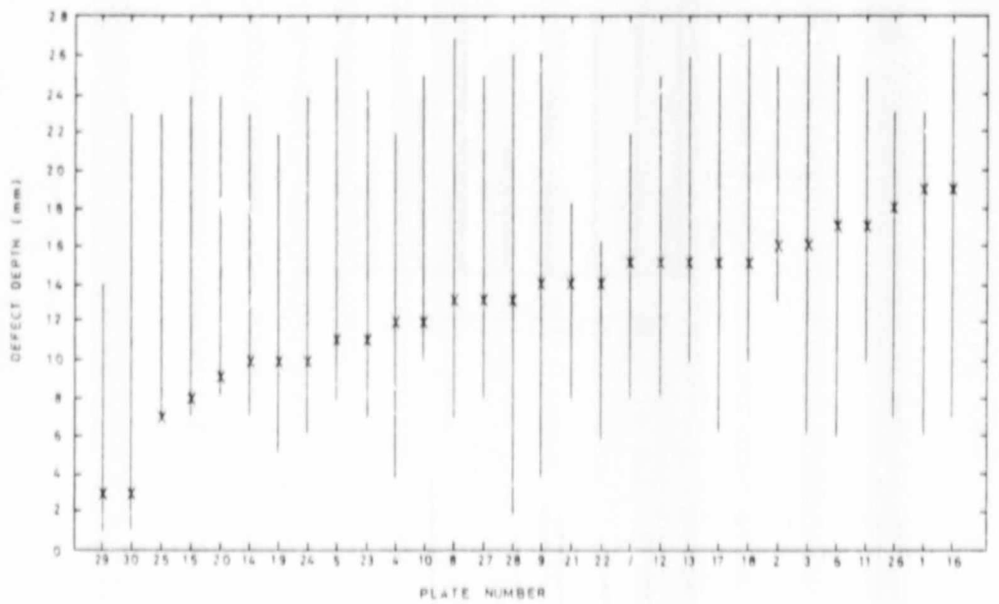


Figure 2.7 The range in UT predictions of defect depths. (Actual defect depth indicated by X).

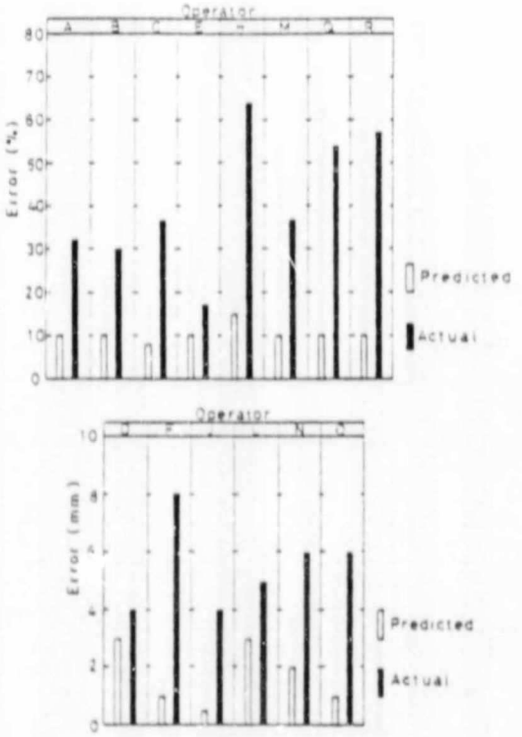


Figure 2.8 The calculated average error of each operator compared to his estimated error on defect heights.

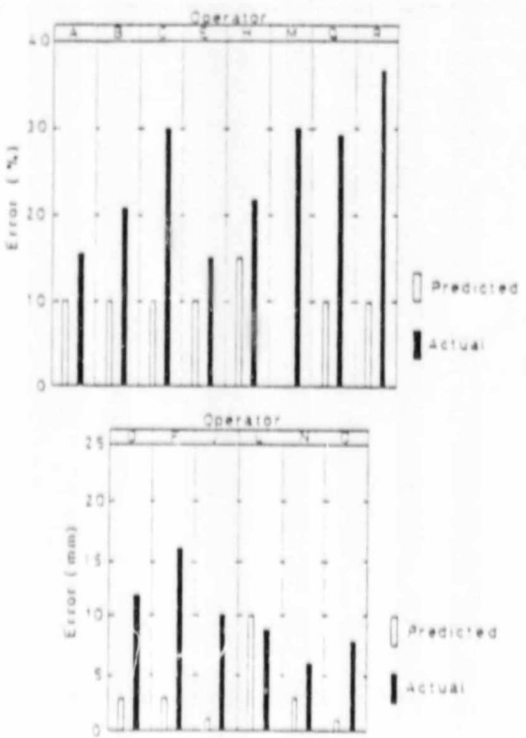


Figure 2.9 The calculated average error for each operator compared to his estimated error on defect lengths.

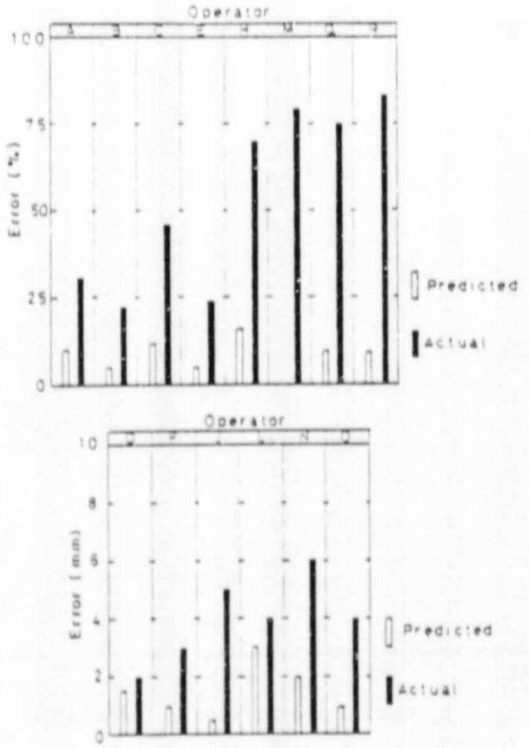


Figure 2.10 The calculated average error of each operator compared to his estimated error on defect depths.

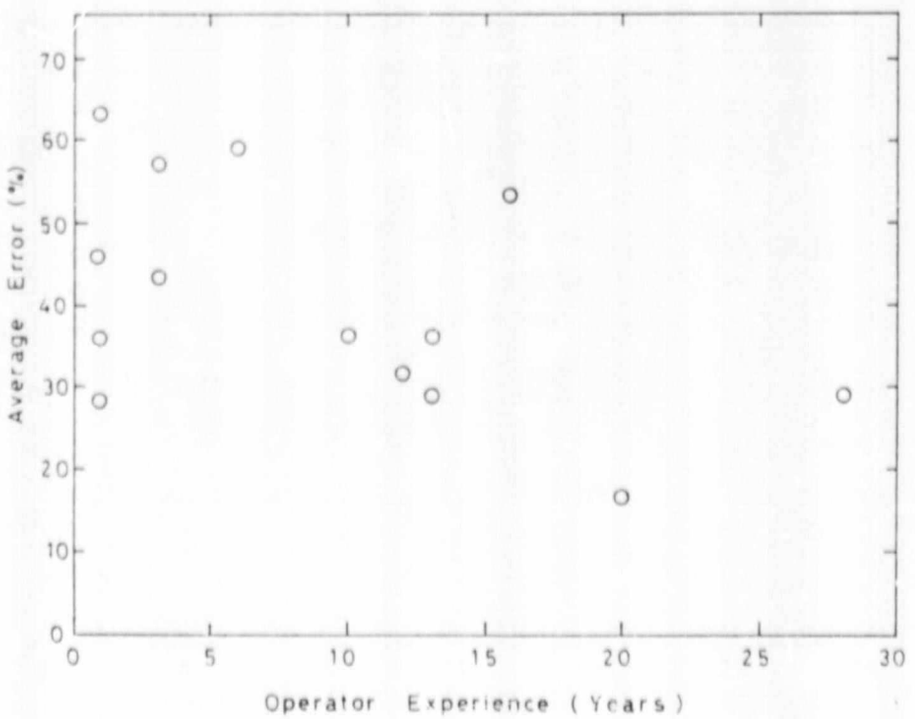


Figure 2.11 The average error in predicting defect heights plotted against the number of years experience of each operator.

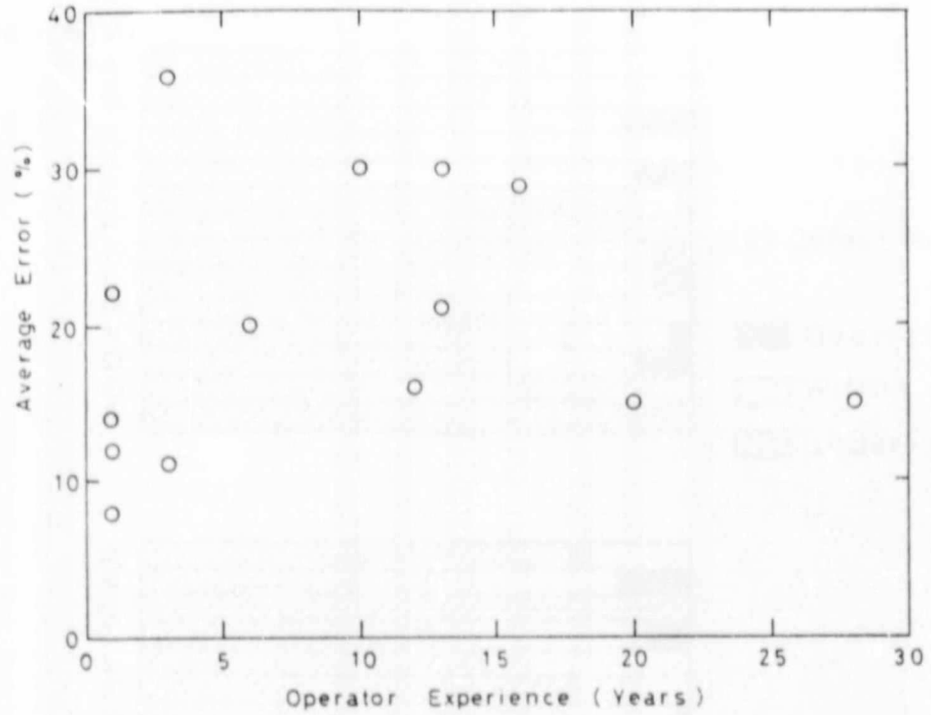


Figure 2.12 The average error in predicting defect lengths plotted against the number of years experience of each operator.

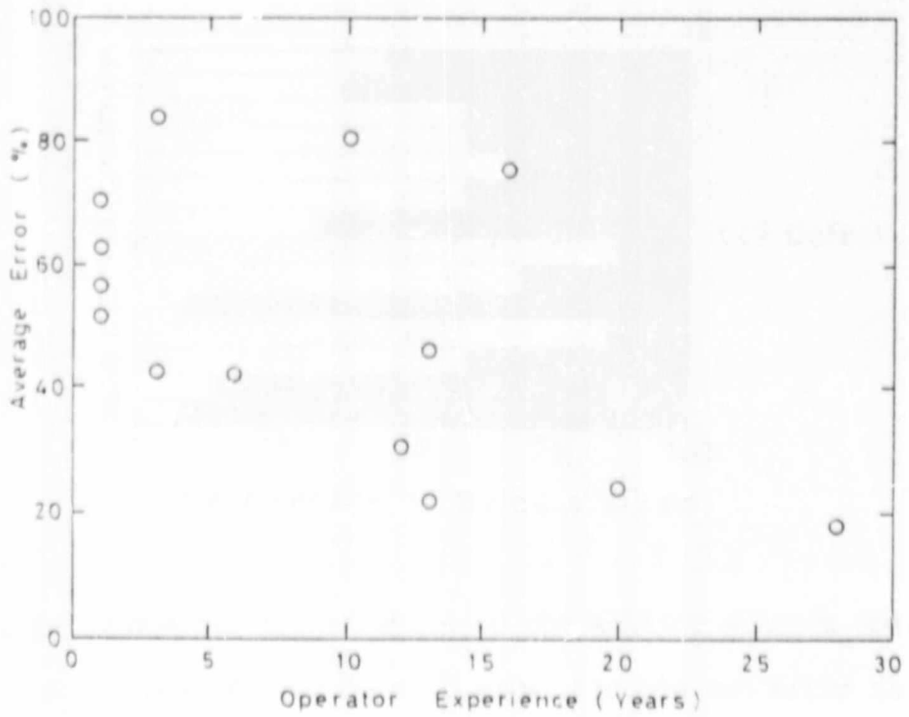


Figure 2.13 The average error in predicting defect depths plotted against the number of years experience of each operator.

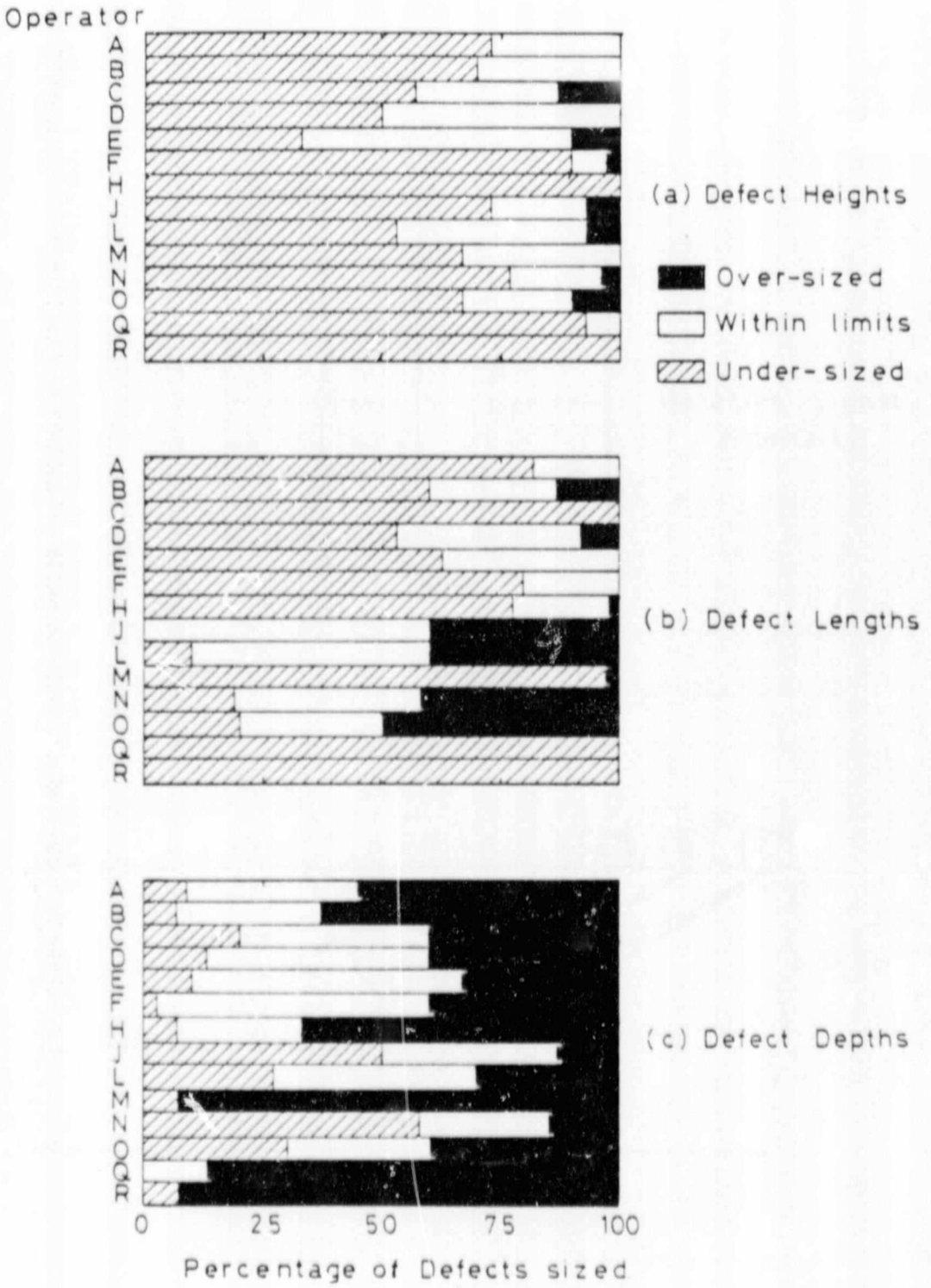


Figure 2.14 Schematic illustration of the ability of each operator to measure the defects to within his own error band. (eg. in the height measurements, operator E undersized 10 of the 30 defects (33%), oversized 3 of the defects (10%) and sized the remaining 17 defects (57%) within his estimated error of ± 10%).

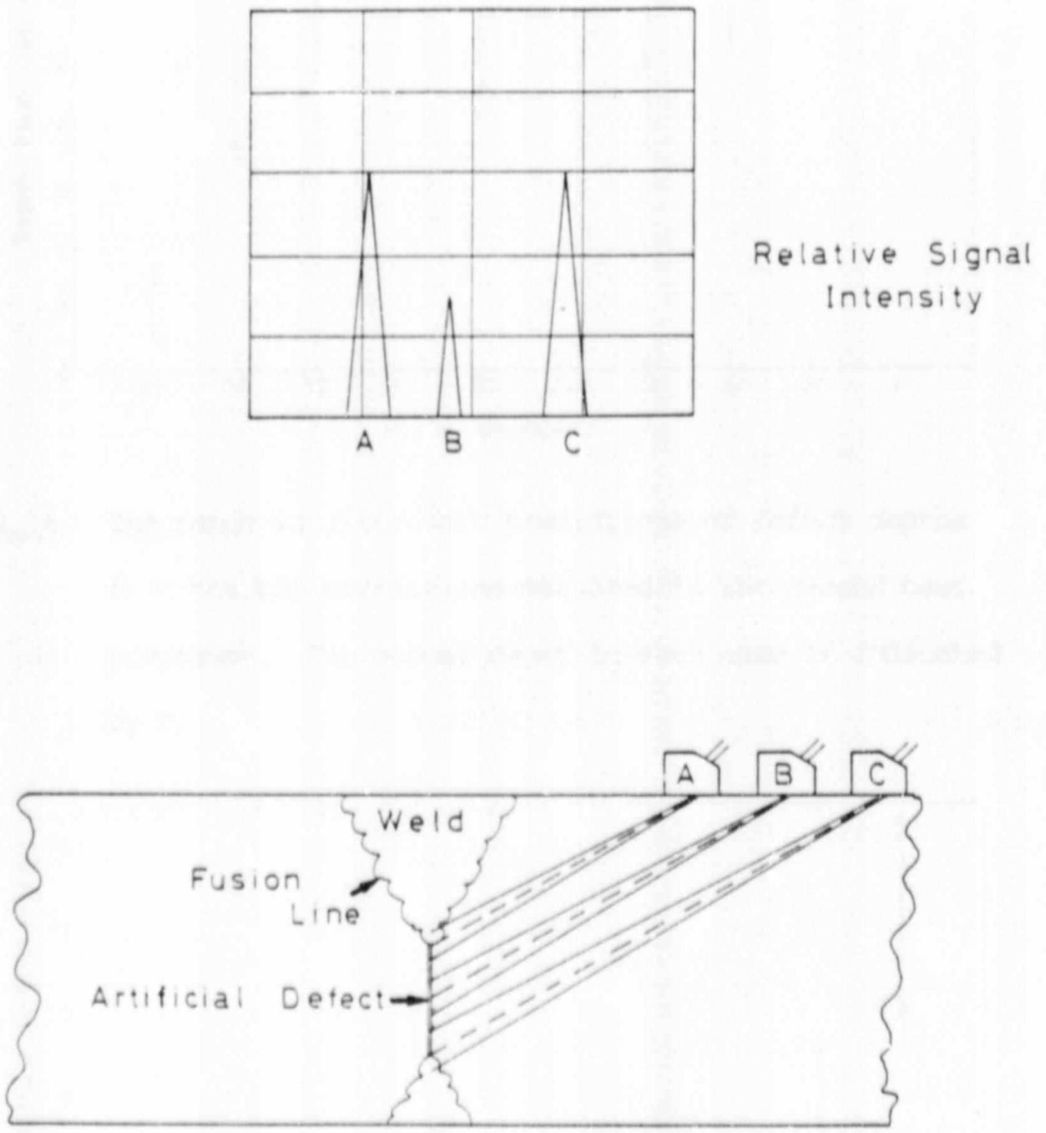


Figure 2.15 A schematic illustrating how the dB drop technique can indicate the presence of two isolated defects rather than a single planar flaw.

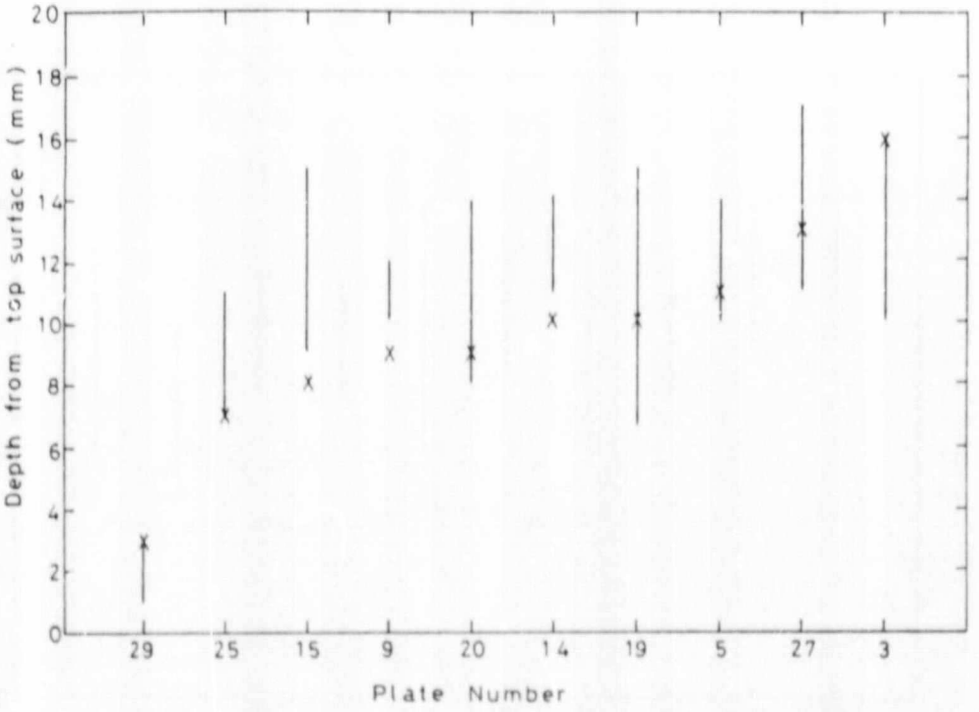


Figure 2.16 The range in ultrasonic predictions of defect depths from the top surface, as measured in the second test programme. The actual depth in each case is indicated by X.

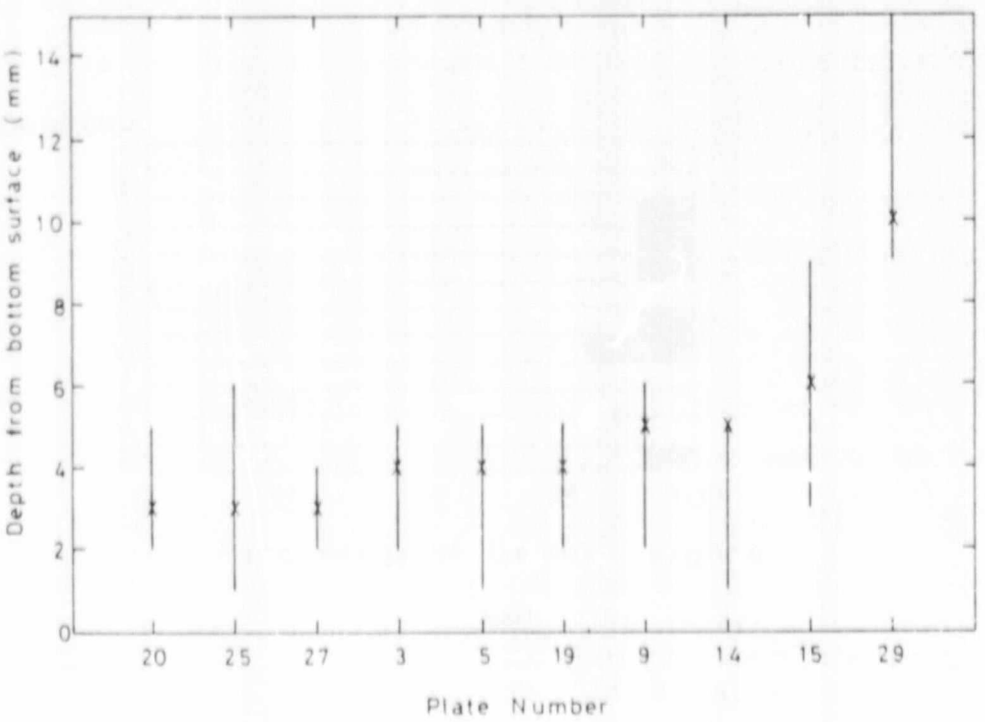


Figure 2.17 The range in ultrasonic predictions of defect depths from the bottom surface, as measured in the second test programme. The actual depth in each case is indicated by X.

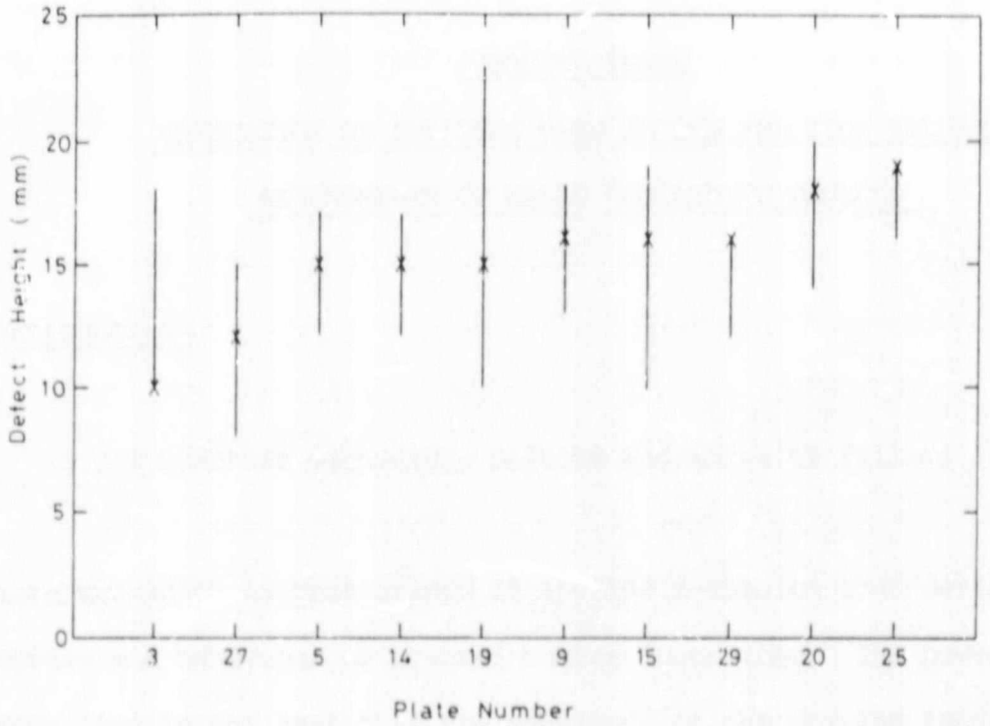


Figure 2.18 The range in ultrasonic predictions of defect heights, as measured in the second test programme. The actual height in each case is indicated by X.

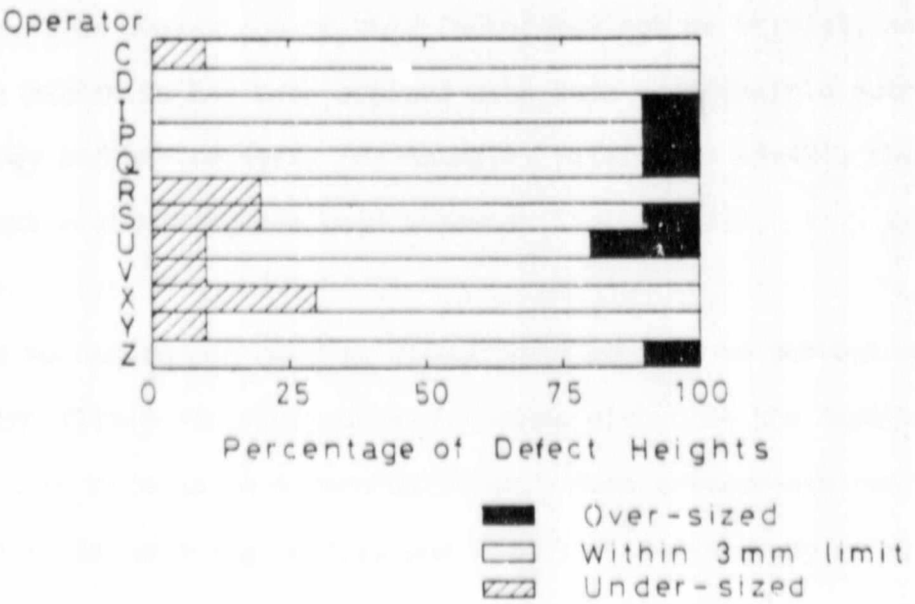


Figure 2.19 A schematic illustrating the ability of the operators to size the defect heights to within 3mm during the second test programme.

CHAPTER THREE

VALIDATION OF ANALYSES USED IN THE FRACTURE MECHANICS ASSESSMENTS OF WELDS CONTAINING DEFECTS

3.1 Introduction

3.3.1 Fracture mechanics, defects and modes of failure

Fracture mechanics is that branch of applied mechanics that deals with the properties and behaviour of cracked bodies under load. The power of the approach lies in the fact that the magnitude of the driving force at the crack tip, or the likelihood of crack extension and therefore failure, can be calculated from easily measureable quantities: the applied stress and the crack length. There is, however, a constant of proportionality, the exact value of which depends on factors such as the crack shape and position, the size of the structural section in which the crack is situated, and the nature of the applied stresses. The evaluation of this factor may not be trivial, and thus whereas fracture mechanics has been applied with some considerable success in high technology industries (see, for example, references 45-49), the widespread use in general engineering has been somewhat limited (45).

Fracture mechanics can be most effectively applied to preventing failures by performing fitness-for-purpose assessments either at the design stage or during service when defects have been detected. Such assessments can consider the criticality of existing or "maximum possible" defects, by relating the defect size to an equivalent critical crack length; alternatively, the optimum material for a given set of operating conditions can be selected. It is important to recognise that there are several modes of failure, and all should be considered at the design stage (50). Thus, mechanical failures can arise from:-

failure by elastic instability (buckling);

failure by excessively large plastic deformation (jamming);

failure gross plastic deformation (yielding);

failure by tensile instability (necking);

and failure by fast fracture (cracking).

Many struc[illegible]fabricated by welding, and the fact that this proces[illegible] can introduce [illegible] various types must obviously be considered during design. In the first four i[illegible]tances of mechanical failure quoted above, the presence of a defect will essentially cause a reduction in the net section, or load-bearing area, thereby reducing the load required to cause failure. It should be noted that buckling may not be entirely dependent on loss of thickness (3), and a more careful assessment should be made, since planar defects lying perpendicular to the applied stress direction would tend to close and hence transmit these stresses. Equally, however, buckling lengths may be reduced if the section ahead of a transverse crack acts as a hinge (51).

In the case of cracking, the defect has a more pronounced effect on failure since it acts as a stress concentrator, and therefore a likely crack initiation site. The mechanism of fast fracture involves the unstable propagation of a crack in a structure, such that once the crack starts to propagate, the loading system produces accelerated growth (50). In addition, fast fractures in service structures have invariably occurred under the action of applied stresses, the magnitude of which are less than the calculated failure stress. These two attributes have emphasized the catastrophic nature of these failures, and has led to the term "brittle failure" being applied. In reality, however, the microscopic crack propagation mechanism can range from cleavage to fully ductile shear separation (50).

3.1.2 Design philosophies and fracture toughness

In assessing the likelihood of failure, engineers can adopt one of two approaches (49,52) and can either consider how the crack starts, or how it

stops. In the first of these approaches, prevention of crack initiation, it is necessary to ensure that the most brittle part of the structure will have a sufficient level of toughness to withstand the maximum stress imposed on it, without allowing any inherent defects to extend in a brittle manner. Crack arrest, on the other hand, allows brittle crack extension to initiate in areas of low toughness, but ensures that the crack will only propagate a short distance until it reaches a region of high toughness, and will then arrest.

Clearly, the safest design philosophy for a welded stucture (53) will be to accept that defects are in fact present, and to design against propagation in all regions of the structure, including the weld metal and heat-affected zone, which are normally less tough than the unaffected parent plate. Unfortunately, however, materials of construction would then be prohibitively expensive, and economic considerations would not allow such an approach. In consequence, therefore, design philosophies follow either the safe-life or the fail-safe approach. In the former, the structure is removed from service at (or before) the end of its design predicted life, so that the possibility of structural failure is eliminated. This can lead to a very safe, but non-economical structure, since the loading conditions and material response to these conditions must be known at all stages during the service history, and large factors of safety are often used. In the fail-safe philosophy, on the other hand, safe-guards are incorporated into the design so that even if local failure occurs, the structure as a whole retains its integrity. One way of providing this redundancy is to use multiple load-path members (54) such that the failure of one member results in a redistribution of the load over the remaining members. Obviously the amount of load reditribution cannot be too severe, or failure may still occur.

Both the safe-life and the fail-safe design philosophies must, of necessity, make use of fracture mechanics in defining either the need to replace damaged portions of the structure, or in calculating the expected fail-safe design life. This means that the fracture toughness of the various materials in the structure

must be evaluated prior to the design. Fracture toughness can be defined as the measurement of resistance to crack extension (55), and there are four commonly used characterising parameters for this material property.

The first is the crack extension force, G, which defines the loss of stress field energy at the crack tip due to the creation of new surfaces as extension occurs. The calculation of this parameter is based on an infinitesimal and virtual increment of new separation area, and can be applied to either stationary or running cracks. Laboratory measurements of fracture toughness, on the other hand, are usually evaluated either in terms of the plane strain fracture toughness, K_{Ic}, the crack tip opening displacement, CTOD, or the J-integral fracture toughness, J_{Ic}. In all three methods, the relevant codes and standards (56-58), stipulate that the fracture toughness be evaluated from a specimen containing a pre-fatigue crack, such that the worst-case fracture toughness can be evaluated.

Each method has conditions that must be satisfied before a valid toughness value can be reported (56-58). Indeed, it is often not possible to report a valid K_{Ic}, due to the size requirements for plane strain, and the material toughness must then be evaluated in terms of the crack tip opening displacement (CTOD) or the J-integral (J_{Ic}). The seemingly obvious implication that any material for which a valid K_{Ic} cannot be obtained is therefore very tough, with a high tolerance to defects, is somewhat misleading. In real structures, thickness effects lead to stress triaxility, and this factor, in addition to possible low temperature operating conditions and high strain rates will act to decrease the toughness of the material. In addition, there are three further reasons for this apparent paradox when dealing with welded structures (45). The first is that the presence of keyways, machined slots and welded joints cause more global stress concentrations, thus increasing the total stress intensity experienced in the region of the defect. The second is that welding residual stresses can locally approach yield stress magnitude, and since these are obviously additive to the nominal applied stresses, the stress required for

brittle failure can therefore be reduced. The third reason relates to the inhomogeniety of the weldment: the wide range of microstructures correspond to a significant variation in material properties exhibited by the weld metal, fusion line, near- and far-heat affected zones and unaffected parent plate. These topics will be discussed further in Chapters Four and Five, to follow.

3.1.3 The BS PD 6493 method for defect acceptance

The British Standard's Published Document, BS PD 6493 (3) gives guidance on some methods for the derivation of acceptance levels for defects in fusion welded joints. It is applicable to welded joints at least 10mm thick in structural and pressure vessel steels, austenitic steels and aluminium alloys. Using this document, the influence of planar and non-planar defects may be assessed for three different modes of failure:-

- brittle fracture;
- fatigue;
- and yielding due to overloading of the remaining cross-section.

Four other failure modes are mentioned, but detailed assessments are not contained in the present document:-

- leakage in containment vessels;
- corrosion, erosion, corrosion fatigue, stress corrosion;
- instability or buckling;
- and creep or creep and fatigue interaction.

To carry out any assessment of flaws on a fitness for purpose basis, it is necessary (3,59) to have detailed information on stresses, defect dimensions, types and positions; and on the material properties, in particular the yield stress and strain, and the fracture toughness. It is then possible to use this reference document either to assess the acceptability of a particular defect located, for example, by non-destructive examination during fabrication or service, or to calculate general defect acceptance levels for particular

components.

The treatment for assessing the effects of flaws on brittle fracture may be carried out on two levels, depending on the level of applied stress. In the case when the applied service stresses are less than the yield stress, the stress intensity (K_I) of the flaw and load combination is calculated, using the procedures set out in the document. If this calculated stress intensity is less than 70% of the plane strain fracture toughness (K_{Ic}) of the material, the defect is considered non-critical.

If, on the other hand, the level of applied stresses exceeds the local yield stress, or if a valid K_{Ic} cannot be obtained from the section thickness under consideration, then a post-yield fracture mechanics assessment is used (3,59). For any defect length, height and depth, an effective defect parameter, $\bar{a}$, is calculated, from Figures 12 and 13 in PD 6493, reproduced here as Figures 3.1 and 3.2. Subject to corrections for free surface effects and aspect ratios, this effective defect parameter is equivalent to the half-length of a through-thickness crack, to the height of a surface flaw, or to half the height of an embedded defect (59). It can be seen from these Figures that variations in the defect length (l) will not have such a pronounced effect on the effective defect parameter as the height (t), or the ligament length (p).

The analysis can then proceed in one of two ways. If, for instance, the level of service stresses have been evaluated, the ratio of the sum of the applied stresses to yield stress is then used in conjunction with the Design Curve, Figure 14 in PD 6493, and reproduced here as Figure 3.3. The value of the constant C extrapolated from this graph can then be used to establish the allowable defect parameter, $\bar{a}_m$. This is then compared to the actual defect parameter, and will indicate whether or not the defect is acceptable. Equally, the actual defect parameter can be used, in conjunction with the material properties, to calculate a value for C as indicated in Figure 3.3. The ratio of applied stress to yield stress that would cause failure can then be obtained

from the Design Curve.

For both treatments, it is necessary to check the stability of the defect, that is, consider the possibility of failure by gross yielding or plastic collapse. This is covered in PD 6493 by detailed procedures which check for "recategorisation" of, for example, an embedded defect to a surface defect, due to net section yield of the remaining ligament. This particular recategorisation procedure is performed using Figure 6(b) in PD 6493, reproduced here as Figure 3.4.

Some care should be taken when translating failure stress ratios to failure stress levels, however, since for small values of C (less than about 0.08), the ratio of applied stress to yield stress will be greater than 2. For applied stresses above yield, the Design Curve approach was derived from ratios of failure strain (3). Clearly, equating stress and strain may give erroneous results when the ratio of applied strain to yield strain is greater than unity, and, by definition, the material is experiencing plastic deformation. The reference document stipulates that when the summation of the maximum principal stresses (excluding residual stresses, but including secondary stresses) exceeds twice the yield stress, the approach must be modified. This may be done (3) by estimating the equivalent applied strain from either elastic/plastic analysis, or experimental results.

Finally, it is worth noting that there is some inherent conservatism when using the Design Curve. It was shown (60) that the constant C has a safety factor of approximately 2 for average behaviour.

3.1.4 The CEGB R-6 elastic-plastic failure assessment

The CEGB R-6 or Two-criteria approach (4) can be applied to any type of structure, but was derived mainly from consideration of ferritic steel pressure vessel components. It deals with treatments of both small scale (or elastic)

and large scale (or plastic) yielding regimes, caters for stresses of a mechanical, thermal and residual nature, and allows for consideration of slow growth. It does not, however, deal with (61):-

arrest of a fast running crack;

time dependant creep effects;

validity and formulation of crack growth laws;

methods of stress analysis;

or impact loading conditions.

In essence, the user of the document calculates two parameters: firstly, an elastic parameter, K_r, which is the ratio of the stress intensity of the flaw and load combination to the plane strain fracture toughness and, secondly, a plastic parameter, S_r, which is the ratio of the applied load to that required to cause plastic collapse. These parameters are then used as coordinates to locate a point on the so-called Failure Assessment Diagram, shown in Figure 3.5. If the point defined by the two parameters lies within the Failure Assessment Line, then the defect is considered safe under the applied loading conditions; if outside, then it is considered critical.

Obviously, this method can be used either to predict the criticality of a known or postulated flaw, or to determine a tolerable flaw size. In the latter case, a range of possible flaw sizes and shapes are used as input data, and the two parameters, K_r and S_r are calculated for the same conditions of applied load and lower bound material properties. These points are plotted on the Failure Assessment Diagram, and the tolerable flaw size is uniquely defined at the intersection between the locus of these points and the Failure Assessment Line.

The Failure Assessment Line was derived by assuming that there are two limits to structural integrity: plastic collapse and linear elastic (or brittle) failure. The Failure Assessment Line, therefore, is an elastic-plastic interpolation, which defines the interaction between these limits. This is intended as a lower

bound criterion to the failure of structures (4), and can only be so if the input data are appropriately chosen. Thus, in calculating S_r a lower bound solution is sought for the plastic collapse loads, and the applied loads are maximised ("worst-case"). Similarily, the lower bound fracture toughness is always used, and the value of the stress intensity should always be an upper bound. In this way, both S_r and K_r are maximised, and when any structure is loaded to failure, the assessment point must lie on or outside the Failure Assessment Line.

In the PD 6493 approach there are inherent conservatisms, but the user of the R-6 document is required to choose his own factors of safety, on the basis of a "sensitivity analysis" (4). This is done in much the same way as establishing tolerable defect sizes, with the exception that all the input data are varied. In this way, the influence of the various input parameters (defect size and position, as well as applied loads and material properties) on the position of the assessment point relative to the Failure Assessment Line can be investigated. Obviously, in marginal situations, where the assessment point lies in the close vicinity of the failure line, a more detailed investigation is essential to yield a more precise estimate of the safety margin.

The original R-6 Failure Assessment Line is independent of material deformation properties, and since real materials tend to strain harden in practice, it may be somewhat conservative. This effect has in fact been investigated and modified Failure Assessment Lines have been experimentally evaluated, based on the strain hardening characteristics of several alloys (61). This point will be discussed in more detail in Chapter Four, to follow.

3.1.5 Summary

This Section has briefly outlined the application of fracture mechanics in determining structural integrity. The various modes of failure have been described, with particular reference to brittle, or fast, fracture. The

fail-safe and safe-life design philosophies were defined, and it was shown that there is some considerable input from fracture mechanics in both of these approaches. Finally, the two widely applied fracture mechanics assessment procedures, the Design Curve approach of BS PD 6493, and the elastic-plastic approach of the CEGB R-6 document were discussed. It was seen that there can be some problems in the PD 6493 approach, when the ratio of applied stresses to yield stress, evaluated from the Design Curve is greater than 2. In the R-6 method, on the other hand, the user is required to perform a sensitivity analysis in order to assess the exact safety margin associated with the failure assessment point defined by the two parameters.

A quantitative description of the longitudinal stress distribution across the thickness in beams subjected to a bending load is more difficult to ascertain than for the corresponding case of uniaxial tensile loading, where the stress is constant throughout the section. In previous work (62,63), the concept of a plastic hinge has been used in defining the stress distribution in the defective welds at the failure load, defined as the maximum load sustained by each specimen. It was considered that this was a reasonable "engineering solution" to the problem at hand, which could only otherwise be solved using finite element methods.

In addition, the defect parameters, weld metal toughness and yield strain were used as input data in the Design Curve approach of PD 6493 to predict the ratio of applied strain to yield strain that would cause failure. For values of applied strain to yield strain less than one, stress and strain are directly proportional, and the failure stress level is then obtained by multiplying the strain ratio by the relevant material yield stress. If, on the other hand, the strain ratio was greater than unity, the failure stress level was then extrapolated from the relevant uniaxial stress-strain curve, obtained from transverse specimens of each weld type (64).

However, these two assumptions could have influenced the overall results of the

reported test programme (62,63). The remaining Sections in this Chapter, therefore, describe the results of a theoretical sensitivity analysis carried out to validate the methods used for the two assessment routes. This sensitivity analysis investigates the effect of changes in the various input data (eg UT predictions of defect height, length and depth) on the calculated failure stress levels and defect criticalities.

3.2 Theoretical Sensitivity Analysis

3.2.1 General approach

As described in Chapter Two, welded test plates, 30 mm thick, were fabricated in a medium strength structural steel using both Manual Metal Arc and Submerged Arc welding techniques. Two sets of test plates were made, one of which contained essentially perfect welds used to obtain the mechanical properties and fracture behaviour of the two types of weldments in both the as-welded and the stress-relieved condition (65). The other specimen set, of thirty test plates, was fabricated that each plate contained a single isolated planar defect (66). Following the previously described ultrasonic inspection, the test plates were subsequently tested to destruction under controlled four point bending in both the as-welded and the stress-relieved condition, with the failure load of each specimen being recorded. Accurate measurements of the defect parameters of length, height and depth were made from the fracture surfaces.

The weld metal properties, measured failure loads, actual defect parameters and ultrasonic data were used quantitatively in conjunction with two widely applied failure assessment procedures, viz. the COD Design Curve approach of British Standard's PD 6493 (1980) (3), and the U.K. Central Electricity Generating Board's Two-Criteria or R-6 Method (1980) (4). The actual failure stress and defect criticality in each test plate were then compared to those calculated on the basis of UT predicted defect sizes. The results of this investigation will be detailed in Chapter Four, to follow.

In the test programme, the defects were machined into the weld preparation as shown in Figure 2.4. The nominal plate thickness was 30 mm, and the specimens were between 80 and 90 mm wide. The defect sizes measured from the fracture surfaces indicated that, although there was a wide range of defect sizes, there were no two identical defects. Furthermore, the defect shape was not precisely reproducible and this would obviously have a significant effect on the stress concentration factor and, therefore, on the fracture behaviour and measured failure loads of each test plate. Thus the real defect sizes could not be used to assess the sensitivity of the analyses used in the test programme (62,63). This was therefore achieved by considering a "typical" reference defect of 10 mm in height, 50 mm in length. This reference defect was located at a depth of 15 mm in a plate section of 30 mm by 100 mm, under an applied bending load of 130 kN. In this work the defect depth was defined as the distance from the top (compressive) surface of the plate to the top edge of the defect. Each defect parameter was then varied in turn, so that the relative effect of <u>each</u> variable on the predictions of failure stress levels and defect criticalities could be investigated.

The weld metal properties used in this validation were those obtained for the MMA and SA weld metals, in both the as-welded and stress-relieved condition (65), as given in Table 3.1. It will be seen that the CTOD corresponding to the attainment of the maximum load plateau (δ_m) is used in this work. The effect of varying this parameter, assuming all other input data to remain constant, is shown in this Chapter. CTOD toughness is a structure-dependent property and assuming a constant stress-strain behaviour, whilst varying the CTOD toughness, is of course an over-simplification of the true situation. However, the <u>critical</u> CTOD toughness for a given material can, conceivably, have one of three values, viz: δ_i, the CTOD at the initiation of crack growth, δ_u the CTOD measured when unstable fracture occurs <u>after</u> stable crack growth and δ_m, the CTOD upon attainment of the maximum load plateau (57). Obviously, the choice of δ_i, δ_u or δ_m as δ_{crit} depends on

the application. If, as in this work, the Design Curve is to be used to evaluate maximum permissible loads, then the use of d_i may be unnecessarily conservative. This has been pointed out previously by the Welding Institute (67).

3.2.2 Assumed stress distribution and calculation of plastic collapse loads.

Figure 3.6 is a schematic diagram of the four point bend system used in the destructive testing of the weldments. Figure 3.7 shows the assumed stress distribution on attainment of maximum load, where it was assumed that a plastic hinge had formed in the thickness of the test plate. Three cases are shown:

(a) the defect is below the neutral axis, in the tensile region;

(b) the neutral axis intersects the defect at some point; and

(c) the defect is above the neutral axis, in the compressive region.

As pointed out in the preceding Chapter, these defects had been fabricated in such a way as to simulate lack of fusion. Preliminary X-ray examination revealed that the defects were "tight" with very little displacement between opposing surfaces, and it was therefore considered that these defects would be able to transmit compressive stresses. Clearly, in all three cases, the critical tensile ligament is within the depth from the bottom of the defect to the bottom of the plate (the extreme tensile fibre). As will be shown later, for a given defect height, the neutral axis has a minimum value when the defect is below the neutral axis, and a maximum when the defect is above the neutral axis. The maximum tensile strain depends on the neutral axis position, and thus in Figure 3.7, case (a) is the most critical condition, and case (c) the least critical.

The application of the plastic hinge concept is theoretically only applicable to elastic-perfectly plastic materials, which can undergo considerable strain at yield without further increase in stress (68). Thus, practical application of

the theory are generally limited to mild steels. However, the tensile properties obtained from transverse weld metal specimens indicated that there was only a slight strain hardening effect after the yield point, and thus the application of the plastic hinge concept was considered justified in this case. The final approximation used involved equating both the tensile and compressive stresses were to the relevant material flow stress, defined as the average of the uniaxial yield stress and ultimate tensile strength

At the fully plastic condition under pure bending, the neutral axis must divide the net load bearing area (A) into two halves. Then, if the centroids of the two halves are a distance $(y_1 + y_2)$ apart, the plastic moment of resistance, M_p is given by:-

$$M_p = \sigma_y \times \frac{A}{2} \times (y_1 + y_2) \qquad (3.1)$$

As outlined above, the plastic theory assumes elastic-perfectly plastic behaviour, and therefore the material flow stress (σ_f) was used, rather than the material yield stress (σ_y). In addition, it is necessary to calculate the distance between centroids, and thus the neutral axis position. This is done by balancing the compressive and tensile forces acting across the section.

Thus, for the stress distribution as shown in Figure 3.7(a), the neutral axis position (depth from the top of the plate, y) was calculated from:-

$$y = \frac{we - Lt}{2w} \qquad (3.2)$$

The plastic moment of resistance is then given by:-

$$M_p = \frac{\sigma_f (we-Lt)}{2} \times \left(\frac{y}{2} + \frac{w h^2 - 2Lt (h-p-t/2)}{2(wh-Lt)} \right) \qquad (3.3)$$

where h is (e-y) and all other parameters are as shown in Figure 3.7(a).

For the case of the neutral axis intersecting the defect, as shown in Figure

3.7(b), the neutral axis position is given by:-

$$y = \frac{be + ce + Lp}{w + b + c} \qquad (3.4)$$

The plastic moment of resistance is given by:-

$$M_p = \frac{\sigma_f (we - Lz)}{2} \times \left(\frac{y}{2} + \frac{w h^2 - L z^2}{2 (wh - Lz)} \right) \qquad (3.5)$$

where $z = (e-y-p)$.

In the final case, where the defect is above the neutral axis, the defective section acts as a homogeneous beam with the neutral axis located at mid-thickness:-

$$y = \frac{e}{2} \qquad (3.6)$$

and the plastic moment of resistance is calculated from:-

$$M_p = \frac{\sigma_f w e^2}{4} \qquad (3.7)$$

Figure 3.8 shows how the distance of the neutral axis (from the top of the beam) will vary for two cases: firstly as the defect height varies between 1 and 20 mm, for a constant ligament of 5 mm; and secondly as the critical ligament varies from 1 to 20 mm, for a constant defect height of 10 mm. (As detailed previously, this reference defect is contained in a rectangular section 30 mm thick and 100 mm wide). It can be seen from this graph that, as the defect height increases, the depth of the neutral axis decreases to a constant value. For the case of a variable critical ligament, the neutral axis position is constant until the defect intersects the neutral axis, and then becomes constant again when the defect is completely above the neutral axis. This is to be expected, because as the defect height increases the top portion of the defect moves into the region of compressive stress (which it can support), and the bottom part of the beam, which is under tension, has a constant area. Thus the load bearing capacity decreases to a minimum, but constant value, dependent on

the size of the critical ligament. In the case of a variable ligament length, there is a constant load bearing area (and therefore constant neutral axis position) until the neutral axis intersects the defect, when the top of the defect moves into the compressive region. Thereafter, the load bearing area increases to a maximum which occurs when the defect is completely above the neutral axis, as in Figure 3.7(c).

The plastic collapse load (P_c) is then given by:-

$$P_c = \frac{M_p}{MA} \qquad (3.8)$$

where MA is the moment arm associated with the four point bending geometry, and is equal to one half the difference between the lower and upper loading spans, as shown in Figure 3.6.

3.3 Results and Discussion

3.3.1 The BS PD 6493 Design Curve Approach.

As described in Section 3.2.1 above, the defect parameters were varied in turn so that the relative effect of changes in these parameters on failure load predictions could be assessed. In each case the defect parameters were used to calculate an effective defect parameter, ($\bar{a}$), from the appropriate diagrams provided in PD 6493 (3). This effective defect parameter, together with the material properties, was then used to predict the ratio of applied strain to yield strain that would cause failure (from the Design Curve in PD 6493, reproduced here as Figure 3.3). The relevant failure stress level was then obtained from a plot of applied stress against strain derived from a conventional tensile test (66). Conditions for ligament stability were checked, and if necessary, the defect was recategorised.

Figures 3.9, 3.10 and 3.11 show the effect on failure stress predictions of

varying the defect parameters of height, critical ligament and length respectively. From Figure 3.9, it is clear that there are two critical defect heights for the assumed situation; the first when the increasing defect height results in plastic collapse of the critical ligament, thus leading to the embedded defect being recategorised as a surface flaw, with a correspondingly lower failure stress. The second critical height occurs when the defect is so large that it results in a brittle failure of the complete section before the ligament can fail by plastic collapse. This therefore accounts for the apparent anomaly, shown in Figure 3.9, of failure stress increasing with increasing defect height.

Similarily, there is a limiting value for the critical ligament, as evidenced in Figure 3.10 where the failure stress decreases slightly with an increasing critical ligament, until brittle failure occurs before plastic collapse of the ligament. This is reflected in an increase in the predicted failure stress. The decrease in failure stress with increasing ligament is due to the "recategorisation" procedure stipulated in PD 6493 where, if plastic collapse occurs, the defect is recategorised as surface breaking, with a height equal to the sum of the height of the embedded defect and the ligament length. Thus as the ligament length increases, for a constant embedded defect height, recategorisation of the defect will result in an increasing height of the effective surface flaw and, therefore, a decreasing failure stress.

Figure 3.11 shows clearly that as the defect length increases, the failure stress level decreases, but only slightly. In this case, the only set of results that were affected by the recategorisation (of the embedded defect to a surface defect) was the as-welded SA material. This is shown by the sharp increase in failure stress when the defect length is increased from 20 mm to 25 mm.

It must be reiterated that the four weld metals used in the investigation only showed a slight strain hardening effect after the yield point. (This is

Author Boothroyd Colin Allistair
Name of thesis Fracture Mechanics Analyses Of Static And Dynamic Failures Associated With Welding. 1986

PUBLISHER:
University of the Witwatersrand, Johannesburg
©2013

LEGAL NOTICES:

Copyright Notice: All materials on the University of the Witwatersrand, Johannesburg Library website are protected by South African copyright law and may not be distributed, transmitted, displayed, or otherwise published in any format, without the prior written permission of the copyright owner.

Disclaimer and Terms of Use: Provided that you maintain all copyright and other notices contained therein, you may download material (one machine readable copy and one print copy per page) for your personal and/or educational non-commercial use only.

The University of the Witwatersrand, Johannesburg, is not responsible for any errors or omissions and excludes any and all liability for any errors in or omissions from the information on the Library website.